Available online at www.sciencedirect.com
SCIENCE DIRECT®
ELSEVIER
Journal of Magnetism and Magnetic Materials 293 (2005) 442–449
Journal of magnetism and magnetic materials
www.elsevier.com/locate/jmmm

Magnetic targeting of aerosol particles for cancer therapy

Javed Ally[a], Benjamin Martin[a], Mir Behrad Khamesee[b], Wilson Roa[c], Alidad Amirfazli[a,*]

[a]*Department of Mechanical Engineering, University of Alberta, Edmonton, Alta., Canada T6G 2G8*
[b]*Department of Mechanical Engineering, University of Waterloo, Waterloo, Ont., Canada N2L 3G1*
[c]*Department of Oncology, University of Alberta, Edmonton, Alta., Canada T6G 1Z2*

Available online 4 March 2005

Abstract

An in vitro model was developed to study and demonstrate the potential and feasibility of magnetically targeted deposition of aerosols for potential applications in lung cancer treatment. Also, a numerical particle tracing model was developed to predict the targeting behavior of the in vitro system; the results from the numerical and experimental studies were in agreement.

Keywords: Magnetic drug targeting; Aerosol drug delivery; Magnetic separation; Lung cancer; Bronchial drug delivery; Model for lung therapy; Simulation; Aerosol distribution; Carbonyl iron particles

1. Introduction

In this study, an in vitro methodology is used to examine the feasibility of targeted delivery of chemotherapeutic agents as an inhaled aerosol to the tracheobronchial region of the lung. In most treatable cases of lung cancer, the cancer occurs in the tracheobronchial region [1]. A numerical model of aerosol particle motion in a magnetic field was also developed to predict the targeting pattern of aerosol particles.

In chemotherapy, cytotoxic drugs are used to kill cancerous cells. These drugs are currently administered intravenously or orally. Generally, combinations of chemotherapy and other drugs are used to mitigate adverse side effects, e.g. skin, gastrointestinal, and bone marrow ailments. Such side effects are inevitable, because the drugs used are toxic to healthy cells as well as cancer cells, and circulate throughout the body.

By delivering chemotherapeutic agents for lung cancer as a magnetically targeted aerosol, it may be possible to reduce adverse side effects by

*Corresponding author. Tel.: +1 780 492 4259; fax: +1 780 492 2200.
E-mail address: a.amirfazli@ualberta.ca (A. Amirfazli).

0304-8853/$ - see front matter © 2005 Elsevier B.V. All rights reserved.
doi:10.1016/j.jmmm.2005.02.038

administering chemotherapy agents directly to the cancerous tissue. With a properly designed magnetic targeting system, the drug particles would be guided to the cancerous tissue by an appropriate magnetic field. The magnetic field also would have to be strong enough to overcome mucociliary clearance. Studies have shown that up to 95% of particles (6.5 μm diameter) deposited in the tracheobronchial region are removed by mucociliary clearance [2].

There is hardly any information available for such a strategy. The only work to the authors' knowledge that has mentioned the concept of using magnetic force to cause site-specific deposition of aerosol particles is an article by Dikanskii and Kiselev [3], where the concept was discussed in the context of nondestructive testing and field visualization. There is no information available in the literature regarding clinical applications, and even in the work of Dikanskii and Kiselev, the methodological aspects are absent.

In contrast to the concept of clinical applications for magnetically susceptible aerosols, magnetically targeted particles administered intravenously have been investigated in the past twenty five years. The works by Lübbe et al. [4] and Goodwin et al. [5] are examples of magnetic targeting in vivo to deliver drug particles to tumors. Others, such as Liu et al. [6], have investigated the use of magnetic particles for blood embolization. Factors affecting magnetic targeting identified in these works, such as fluid flow velocity, field gradient, and magnet positioning, should also be considered for aerosol targeting.

The first step in the development of a magnetic targeting system for lung cancer is to characterize the deposition of aerosols in simulated conditions of the tracheobronchial region. This was done in vitro using a bench top model. In order to facilitate future development of the system, a numerical simulation of particle deposition was also developed and verified using the experimental results. The current work represents a necessary initial step in the development of a magnetic targeting system, and as such, the fundamentals and possibilities of targeted deposition and retention of magnetic aerosol particles in an idealized model representing the conducting airways is considered.

2. Theoretical background

Inhaled aerosols consist of fine particles suspended in air: the flow of air around the particles is characterized by the particle Reynolds number, *Re*. The Reynolds number describes the ratio of the magnitudes of the inertial and viscous forces on the particle. For small Reynolds numbers ($Re<0.5$), the drag force, $\vec{F}_{\mathrm{D}}$, on a particle is purely due to viscosity, and can be calculated using the Stokes expression for drag force on a sphere as

$$\vec{F}_{\mathrm{D}} = 3\pi\mu d(\vec{v}_f - \vec{v}_{\mathrm{p}}), \tag{1}$$

where μ is the viscosity of air, d is the particle diameter, $\vec{v}_f$ is the air velocity, and $\vec{v}_{\mathrm{p}}$ is the particle velocity. For the air flow (0.34 m/s) and particles (1–3 μm diameter) used in these experiments, the particle Reynolds number was less than 0.1, so the Stokes drag equation shown was applicable.

The magnetic force, $\vec{F}_{\mathrm{M}}$, on a small sphere in a nonmagnetic fluid can be calculated as

$$\boldsymbol{F}_{\mathrm{M}} = \tfrac{1}{2}\mu_0\chi V_{\mathrm{p}}\nabla(\vec{\boldsymbol{H}}^2), \tag{2}$$

where μ_0 is the permeability of free space, χ is the magnetic susceptibility of the particle, V_{p} is the particle volume, and $\vec{\boldsymbol{H}}$ is the magnetic field intensity [7].

In aerosols, the density of the particles is typically much higher than that of air, so the buoyancy force can be neglected. Lift is also neglected, as the air velocity can be assumed constant over the particle diameter. Consequently, application of Newton's second law yields the following force balance for a particle:

$$m\frac{\mathrm{d}\vec{v}_{\mathrm{p}}}{\mathrm{d}t} = \vec{\boldsymbol{F}}_{\mathrm{M}} + m\vec{\boldsymbol{g}} + \vec{\boldsymbol{F}}_{\mathrm{D}}, \tag{3}$$

where m is the particle mass, $\vec{\boldsymbol{g}}$ is acceleration due to gravity, and $\vec{\boldsymbol{v}}_{\mathrm{p}}$ is the velocity of the particle. Substituting Eqs. (1) and (2) into Eq. (3) and considering $m/\rho_{\mathrm{p}} = V_{\mathrm{p}}$ and $\nabla(\vec{\boldsymbol{H}}^2) = 2\vec{\boldsymbol{H}}\nabla\vec{\boldsymbol{H}}$ results in the following expression:

$$\frac{m}{3\pi\mu d}\frac{\mathrm{d}\vec{\boldsymbol{v}}_{\mathrm{p}}}{\mathrm{d}t} = \frac{m}{3\pi\mu d}\left(\frac{\mu_0\chi}{\rho_{\mathrm{p}}}\vec{\boldsymbol{H}}\nabla\vec{\boldsymbol{H}} + \vec{\boldsymbol{g}}\right) + (\vec{\boldsymbol{v}}_f - \vec{\boldsymbol{v}}_{\mathrm{p}}), \tag{4}$$

where ρ_p is the particle density and t is time. Defining a time constant τ as $m/3\pi\mu d$, the equation of motion for a single particle can be written as

$$\tau\frac{d\vec{v}_p}{dt} = \tau\left(\frac{\mu_0\chi}{\rho_p}\vec{H}\nabla\vec{H} + \vec{g}\right) + (\vec{v}_f - \vec{v}_p). \quad (5)$$

In the numerical model developed, described in the next section, the motion of a particle is analyzed by discretization into small elements. For a single element, $\vec{H}\nabla\vec{H}$ can be taken as a constant. The fluid velocity can similarly be assumed constant over an element. The solution to Eq. (5) over an element is thus

$$\vec{v}_p = \left[\vec{v}_f + \tau\left(\frac{\mu_0\chi}{\rho_p}\vec{H}\nabla\vec{H} + \vec{g}\right)\right](1 - e^{-t/\tau}) + \vec{v}_{p,0}e^{-t/\tau}, \quad (6)$$

where $\vec{v}_{p,0}$ is the initial velocity of the particle. For a 1 μm iron particle in air at standard temperature and pressure, $\tau = 0.024$ ms; the time steps used in the numerical model were 1 ms, two orders of magnitude larger. Therefore, the time dependent terms in Eq. (6) can be neglected, and the particle velocity is given by Eq. (7):

$$\vec{v}_p = \vec{v}_f + \tau\left(\frac{\mu_0\chi}{\rho_p}\vec{H}\nabla\vec{H} + \vec{g}\right). \quad (7)$$

The second term Eq. (7) represents the magnetic and gravitational forces on the particle, and is proportional to d^2 since $\tau = m/3\pi\mu d = (\rho_p/18\mu)d^2$.

3. Numerical model

A particle tracing code was developed to predict the trajectories of an initial distribution of particles representing the particle distribution in the experiments. The trajectories of the particles over discrete time steps of 1 ms were established using the second order Runge–Kutta method. The particle velocity $\vec{v}_p(\vec{x})$ was calculated using Eq. (7) with values of $\vec{H}$, $\nabla\vec{H}$ and $\vec{v}_f$ at each position $\vec{x}$. The magnetic field strength $\vec{H}$ was determined using finite element analysis, described below. The fluid velocity $\vec{v}_f$ was determined experimentally (see next section) and used as input for the code. The trajectories were used to predict the collection efficiencies of the magnets used in the experiments.

Finite element analysis was performed using the ANSYS finite element package to determine the magnetic field for the apparatus. Ten node quadratic tetrahedral elements were used to solve for the magnetic scalar potential at the nodes. The field intensities at the element centroids were computed by taking the gradient of the magnetic scalar potential numerically. The permanent magnets (25.4 mm diameter, 3.2 mm thick neodymium-iron-boron) were modeled in a 100 mm × 200 mm × 500 mm air volume (see Fig. 1). The size of the air volume required to obtain accurate results was determined by comparing results of the finite element analysis with different air volume sizes to flux values measured for a single permanent magnet (see Fig. 2). Magnetic flux measurements were performed with a gaussmeter (F.W. Bell Model 5080).

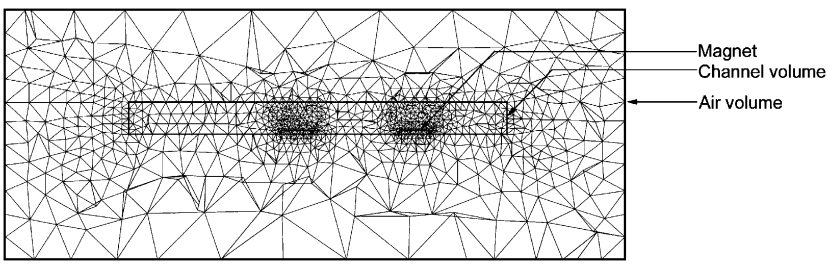

Fig. 1. Finite element mesh for the experimental apparatus in the two permanent magnet configuration.

A 25 mm × 50 mm × 300 mm air volume was defined within the larger air volume (see above) to represent the aerosol channel of the experimental apparatus (see Fig. 1). At the upper surface of the smaller volume, where the magnetic field gradient is small, element size was 10 mm. At the surface of the magnets, 0.5 mm elements were used. In a cylindrical region around the magnets, 50 mm in diameter and 50 mm high, the element size was set to 2 mm. The small element sizes near the magnets were necessary to accurately model the large field gradient near the magnet.

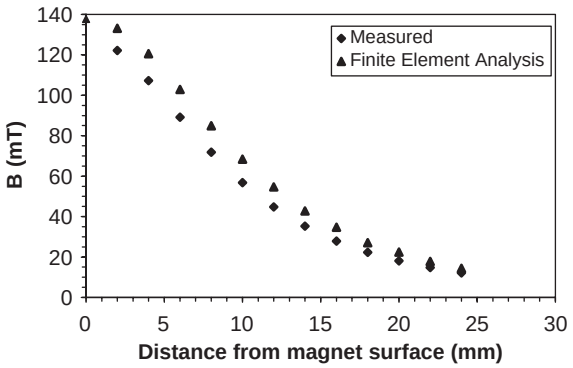

Fig. 2. Comparison of finite element results and measured values for magnetic flux perpendicular to permanent magnet face along center axis.

The magnetic field strength calculated using finite element analysis is used in the particle tracing code to determine the velocity at each particle position. For each position, the code searches the finite element results to locate the four points closest to the particle position. The magnetic field strengths at these points were used to calculate the magnetic field strength by interpolation, and to determine the field gradient at the particle position.

4. Experimental model and methodologies

The airways in the tracheobronchial region consist of a series of branching tubes, the largest being the trachea (approximately 25 mm in diameter). The typical air speed in the trachea is 0.4 m/s [8]. The tubes are lined with a cellular epithelium containing glands that secrete a 5–10 μm thick layer of mucus that is moved up the airway by cilia in order to remove foreign particles.

The above physiological system was modeled by flows of air and water in opposite directions inside of an acrylic channel (25 mm × 50 mm, 300 mm long, see Fig. 3). Deposition of particles in the channel due to gravity was thus negligible, since the length of the channel is much less than the

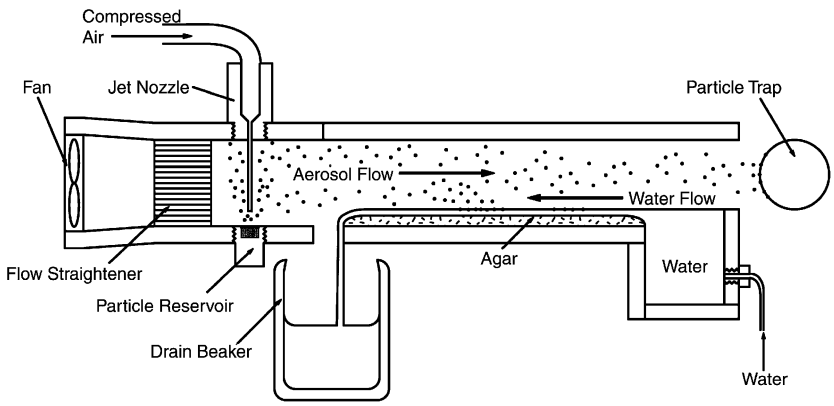

Fig. 3. The experimental apparatus. The apparatus consists of an acrylic channel, 25 mm × 50 mm, 300 mm long. The aerosol was generated using a 95 m/s jet of compressed air from a 17 Ga. needle, and the particles entrained in the air flow produced by the fan. The particle trap consisted of a 75 mm long, 25.4 mm internal diameter copper tube with permanent magnets inside. A 0.1 mm/s flow of water atop an agar bed at the bottom of the channel was used to simulate mucus flow. The water flow was produced by a peristaltic pump.

average settling distance due to gravity, i.e. 3.8 m for the particles used (1–3 μm carbonyl iron spheres from Alfa Aesar). The particles could correspond to the magnetic cores of 6–10 μm therapeutic particles with polymer shells.

The aerosol was produced by deagglomeration of iron particles, using jet of air [9], which were entrained in the main flow of air produced by a fan (see Fig. 3). Those particles that did not deposit in the channel were caught at the end by a particle trap, whereas particles deposited in the channel and removed by the water flow were caught in a beaker. The water was allowed to flow for 15 min after the aerosol was passed through the channel in order to see if any particles were removed. By collecting all of particles that passed through the channel, the collection efficiency of the magnets could be determined.

The agar bed served two purposes: to facilitate the flow of water as a thin film, since agar is very hydrophilic, and to facilitate measurement of the amount of particles deposited in the channel. After each experiment, the agar in the channel was divided into four sections. Each section was carefully removed to avoid loss of particles and placed in a beaker of water. The beakers were heated on a hot plate until the agar melted. The iron particles were held in the beaker with a permanent magnet as the water and melted agar were poured out. The particles were then rinsed, dried, and weighed using an analytical balance (Sartorius Model BL210S, 0.1 mg resolution). The particles from the particle trap and drain beaker were washed into beakers, separated, and weighed similarly.

The air velocity profile in the channel (Fig. 4) was measured using particle doppler anemometry. The air flow was made laminar using a flow straightener. The disruption of the velocity profile due to the jet used to disperse the aerosol particles was assumed to be the minimal. The air flow in the channel from the fan was 0.47 L/s, whereas the air flow from the jet was 0.08 L/s for 0.2 s, increasing the air flow by only 3% over one second. The velocity of the air at each particle position was determined by interpolating from the velocity profile (Fig. 4). The mucus clearance mechanism was simulated with a 0.1 mm/s flow of water atop

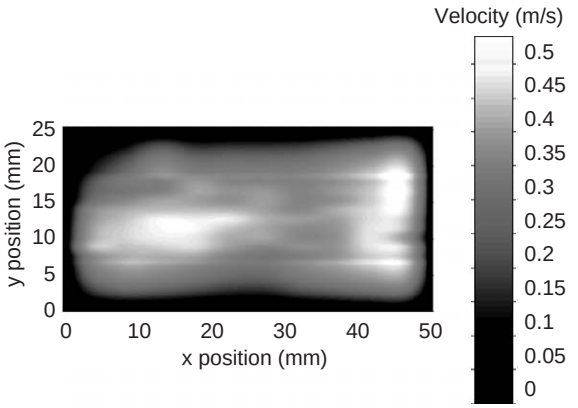

Fig. 4. The velocity profile over the 25 mm × 50 mm cross section of the channel. The velocity profile was measured using particle doppler anemometry. This measurement technique uses laser beams to measure the velocity of a fine mist of water droplets in a flow at a given point; the droplets follow the streamlines of the flow. The velocity profile measurements showed that at all points the velocity was parallel to the long axis of the channel. The average velocity was 0.34 m/s. The velocity profile was the same along the length of the channel.

an agar bed (see Fig. 3). In reality, the flows of air and mucus are much more complex. The simplifications described were made to examine the parameters affecting aerosol deposition, and for verification of the numerical model.

Using the setup described above, two sets of experiments were conducted. In the first set, the magnetic field was applied using electromagnets in a magnetic circuit; the channel was placed between the pole pieces of the circuit, as shown in Fig. 5a. In the second set of experiments, permanent magnets were placed in the channel underneath the agar layer, as shown in Fig. 5b.

5. Results and discussion

Collection efficiencies were calculated for each section of the apparatus. The collection efficiency for a section was defined as the percentage of the total particles deposited in the section. The collection efficiency for each experimental configuration was averaged over three replicate experiments; the results are shown in Fig. 6a. The sections of the apparatus were numbered as

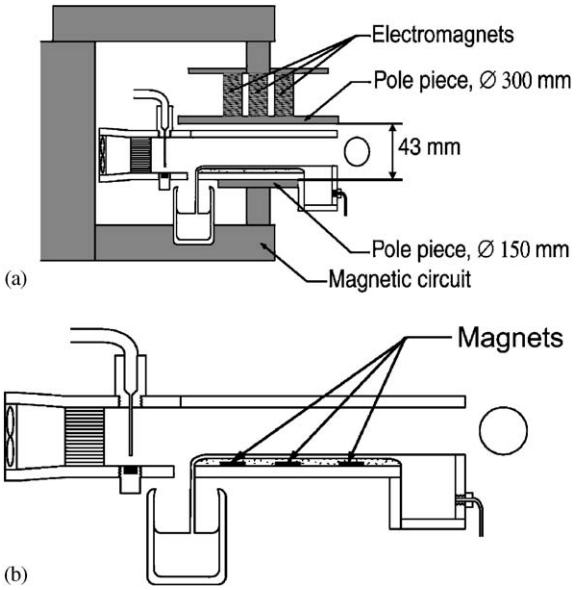

Fig. 5. (a) The experimental apparatus in between the pole pieces of the magnetic circuit. The three permanent magnets had a magnetomotive force of 4000 ampere-turns, with 35 mm diameter 1018 steel cores. The magnetic circuit was also made of 1018 steel, and had a square cross-sectional area of 2500 mm^2. (b) The experimental apparatus with permanent magnets (3 permanent magnet configuration shown). The magnets were 25.4 mm diameter, 3.2 mm thick neodymium-iron-boron magnets.

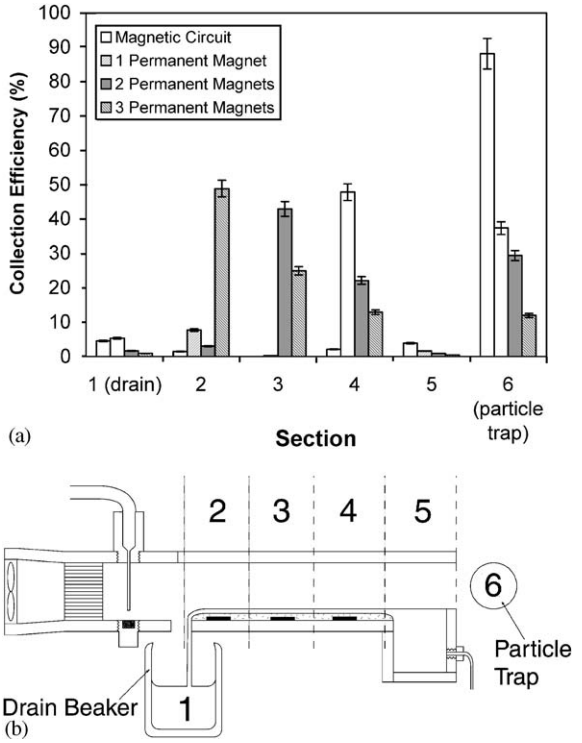

Fig. 6. (a) Experimental particle collection efficiencies for each channel section. Collection efficiency for Section 3 in the magnetic configuration was 0%. In the single permanent magnet configuration, the magnet was placed in Section 4. In the two magnet configuration, the magnets were in Sections 3 and 4. In the three magnet configuration the magnets were in Sections 2–4. (b) Channel section numbering (3 permanent magnet configuration shown).

shown in Fig. 6b. In the magnetic circuit configuration, less than 10% of the particles were retained in the channel. With the permanent magnet configurations, overall collection efficiency of 48–87% were achieved (collection efficiency depended on the number of magnets used. The graph in Fig. 6a shows the collection efficiency for each section (see Fig. 6b).

The collection efficiencies predicted numerically corresponded within 12% of the experimental results in the three magnet configuration. For the two magnet configuration, the predicted collection efficiency corresponded within 10%, and for a single magnet, within 4%. The numerically predicted collection efficiencies were based on the trajectories of 900 particles, 1–3 μm in diameter, distributed over the cross section of the channel entrance. Fig. 7 shows that collection efficiencies predicted using the numerical model tended to be less than the actual collection efficiencies. Particle coagulation was a likely source of error in the numerical results. In the experiments, particle aggregates could have been produced by collisions in the aerosol flow, or by particles adhering in the particle reservoir before deagglomeration. The aggregates would have larger effective diameters than single particles, causing the particle tracing code to underestimate the magnetic force on some of the particles (see Section 2). An explanation for the larger deviations between the numerical and experimental results in the two and three magnet configurations is that the error may be due to the formation of larger (coagulated) particles in the aerosol due to the magnetic field. Preferential deposition of the larger particles in Section 3 for

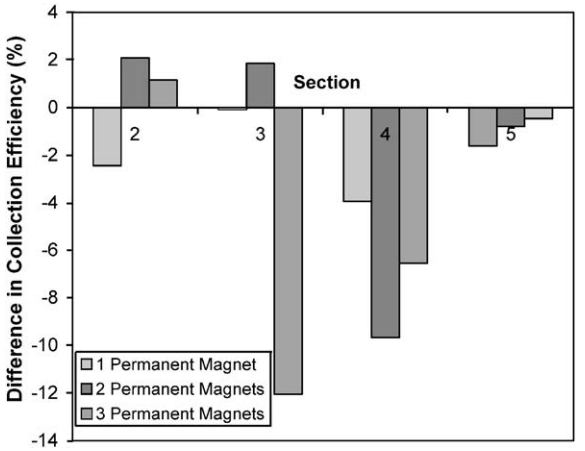

Fig. 7. Numerical minus experimentally determined collection efficiencies for sections in the channel in the three permanent magnet configurations.

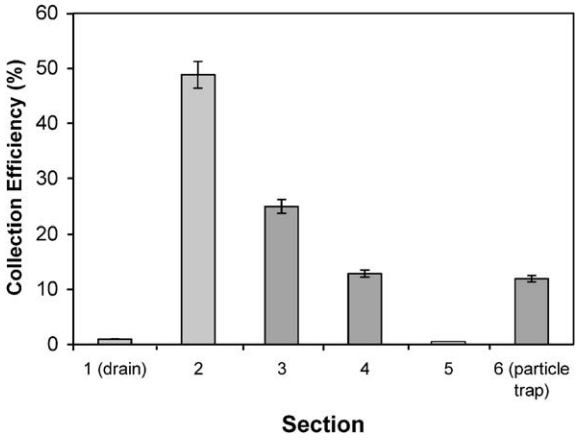

Fig. 8. Collection efficiency results in the three magnet configuration. The total collection efficiency for the three permanent magnet configuration was 87%.

the two magnet configuration and Section 4 for the three magnet configuration would produce the observed deviation from the numerical results.

The difference in the collection efficiencies between the permanent magnet and magnetic circuit results illustrates the importance of the magnetic field gradient. The collection efficiency for a single permanent magnet was 20 times that of the magnetic circuit, despite the size of the bottom pole piece (150 mm diameter) being much larger than the size (25.4 mm diameter) of a permanent magnet. At the midpoint of the channel away from the edges of the pole pieces, the magnetic field strength was 36 mT. At the same point above a permanent magnet, the field strength was 45 mT, only 10 mT higher. The field gradient for electromagnet was 0.03 mT/mm, while for the permanent magnet the field gradient was 3 mT/mm, 100 times higher, which made the single permanent magnet more effective than the magnetic circuit.

The results show that the overall collection efficiency for the channel increases with more permanent magnets. The individual collection efficiency of each added magnet decreases, however (see Fig. 8). This is because the particle concentration of the aerosol decreases as particles are deposited. This is clearly illustrated in the numerical results shown in Fig. 9; it shows that the particle concentration in the region near

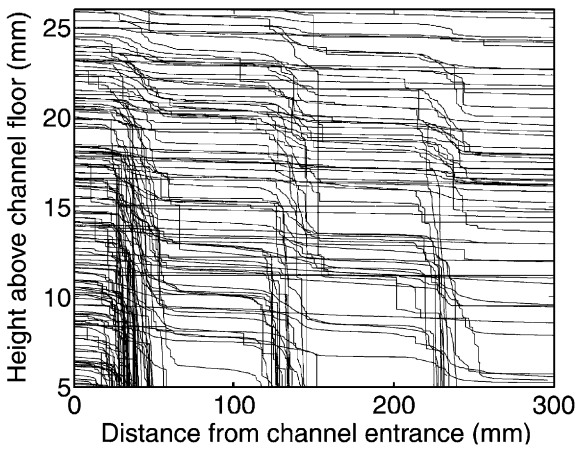

Fig. 9. Particle trajectories (shown with hairline trace lines) as predicted by the particle tracing code for the three magnet configuration. Nine hundred particles with diameters from 1 to 3 μm are distributed randomly along the cross section of the channel entrance. Two hundred seventy-seven particles left the channel uncaptured, representing a 69% collection efficiency predicted numerically.

the magnets decreases along the channel length, i.e. the number of particles available for deposition is reduced (fewer trace lines seen in Fig. 9 as distance from the channel entrance increases). Fig. 9 also shows that the particle concentration decreases more in the lower half of the channel where the magnets are placed than in the upper

half, i.e. fewer trace lines are seen in the bottom half of Fig. 9 after ~150 mm along the channel compared to the upper half.

Overall, the results of this model study show promise in application of magnetic targeting for aerosolized delivery of chemotherapeutic agents; it demonstrates in principle the potential of such strategy, for the first time, to target aerosolized drugs for lung cancer treatment. These results give insights into the design requirements for a magnetic aerosol targeting system. A high magnetic field strength and gradient is desirable for this purpose. The high-gradient region of the magnetic field should be as large as possible. The particle concentration should also be considered. To maximize the collection efficiency, particles should be removed from all regions of the aerosol flow, for example by applying the magnetic field from various directions. Of course further studies to address the effects of fluid flow, e.g. as a result of coughing or geometry of the airways should be studied. Plans are to represent a more realistic mucociliary clearance mechanism by using frog palates. Regarding the numerical study, Eq. (2), can be modified using various correction factors to account for Brownian motion of particles less than 1 μm in diameter, as well as for nonspherical particles, particle clusters, and wall effects. These corrections could be used to extend working conditions of the numerical model beyond those of this investigation and result in better agreement between the experimental results and numerical predictions.

6. Conclusions

The results of this investigation demonstrate in vitro the possibility of magnetically targeting aerosols for chemotherapy. Magnetically targeted site-specific deposition was achieved, and the deposited particles were not removed by the simulated clearance mechanism. The particles used, 1–3 μm iron spheres, could correspond to the ferromagnetic cores of therapeutic particles. A numerical model was also developed to predict the trajectories of the aerosol particles. The numerical model was validated using the experimental results. The results of the experiments showed that magnetic field gradient and aerosol particle concentration are important considerations for magnetic targeting of aerosols.

Acknowledgements

The authors gratefully acknowledge support of the Alberta Cancer Board, NSERC, and REE, University of Alberta.

References

[1] H. Spencer, Pathology of the Lung, fourth ed., Pergamon Press, Oxford, 1985.
[2] G. Scheuch, W. Stahhofen, J. Heyder, J. Aerosol Med. 9 (1996) 35.
[3] Y.I. Dikanskii, V.V. Kiselev, Magnetohydrodynamics 34 (1998) 212.
[4] A.S. Lübbe, C. Alexiou, C. Bergemann, J. Surg. Res. 95 (2001) 200.
[5] S. Goodwin, C. Peterson, C. Hoh, C. Bittner, J. Magn. Magn. Mater. 194 (1999) 132.
[6] J. Liu, G.A. Flores, R. Sheng, J. Magn. Magn. Mater. 225 (2001) 209.
[7] R. Gerber, R.R. Birss, High Gradient Magnetic Separation, Research Studies Press, England, 1983.
[8] W.H. Finlay, The Mechanics of Inhaled Pharmaceutical Aerosols: An Introduction, Academic Press, London, 2001.
[9] Z.L. Wang, C.F. Lange, W.H. Finlay, Int. J. Pharm. 275 (2004) 123.